Estimating Groundwater Recharge and Precipitation Sources of the Zamora River Basin, Southeastern Ecuador, by Using GIS and Stable Isotopes

Alexander Gualli
Universidad Regional Amazónica Ikiam
Paulo Galvão
Federal University of Minas Gerais
Mayra Buenaño
Ministerio del Ambiente Agua y Transición Ecológica
Bruno Conicelli (bconicelli@gmail.com)
Universidad Regional Amazónica Ikiam

Research Article

Keywords: Groundwater recharge, GIS, water balance, stable isotopes, conceptual model

Posted Date: August 9th, 2023

DOI: https://doi.org/10.21203/rs.3.rs-1851102/v1

Abstract

The correct management of groundwater depends on information regarding the evolutionary processes of groundwater and the characterization of spatial variability of recharge mechanisms. GIS-based index models have become a reliable alternative for mapping and interpreting recharge models due to their adaptability and reliability in estimating recharge. Furthermore, stable isotopes of hydrogen and oxygen in water (δ^2H and $\delta^{18}O$) help determine the origin and monitoring of water in the hydrological cycle. This paper aims to contribute to the knowledge of groundwater recharge by developing a conceptual recharge model using stable isotopes and estimating the recharge amount using a spatially distributed water balance model based on GIS for the Zamora River Basin (ZRB) in Ecuadorian Amazon. Due to the basin's size and geography, it was necessary to divide it into six precipitation blocks. The high precipitation rates resulted in high (18.22%) and moderate (30.93%) recharge zones across the basin. The analysis of stable isotopes in water indicates that precipitation water comes from the east, from the Amazon plain. In the valleys, precipitation enriched in $\delta^{18}O$ suggests that it has undergone a recycling process in the basin; groundwater recharge comes from these precipitations. This analysis provides a simplified representation of reality that can assist in predicting the impacts of human activities on the basin.

1. Introduction

Understanding groundwater recharge is crucial for effective water resources management (Healy & Scanlon, 2011). Groundwater recharge is a hydrologic process where water from unsaturated zones infiltrates into saturated zones below the water table's surface (Freeze & Cherry, 1979). Several factors, such as topography, lithology, geological structure, porosity, soil cover, and climate, can affect groundwater occurrence and movement (Fenn et al., 1975). Therefore, groundwater and aquifer research require in situ (hydro)geological experiments and geophysical research that help explain the groundwater replenishment process and help evaluate temporal and spatial differences in groundwater flows in the study area (Yeh et al., 2014).

Different methods can estimate groundwater recharge, but none is uncertainty-free (Scanlon et al., 2002). Direct field measurements such as groundwater level measurements, aquifer tests, or surface water flow measurements do not represent the entire aquifer (Hendrickx, 1992). Darcy equation-based methods require field measurements and numerical methods that use groundwater flow equations under full or partial saturation (Andreo et al., 2008). There are also methods based on natural tracers, such as naturally dissolved compounds like chloride balance, or artificial tracers such as organic and inorganic dyes (Wood, 1999; Mazor, 2004). However, natural tracers may offer only indirect measurements of groundwater recharge, and the infiltration mechanism may affect the interpretation of results (Allison, 1988).

Another way to estimate groundwater recharge is the use of water balance methods. The water input can be equal to the amount discharged plus the variation in the volume of stored water (Scanlon et al., 2002). Water balances can be estimated using semi-empirical equations based on actual precipitation and temperature measurements, calculating indirect directions of existing and potential evapotranspiration and rainfall (Thornthwaite & Mather, 1955). The water balance approach allows for estimating recharge rates for a large aquifer, such as at the scale of a basin (Galvão et al. 2018). The Thornthwaite & Mather method calculates potential evapotranspiration (PET) from monthly and annual heat indices as a function of air temperature, corrects the PET value to Actual Evapotranspiration (AET) from PET, as well as precipitation data and field capacity (capacity of the soil to hold water before percolation). Once the AET is calculated, runoff and infiltration values can be estimated (Galvão et al., 2018).

Regarding the estimation of groundwater recharge on a regional scale (basin dimensions), some studies use flow measurements and numerical models (Nolan et al., 2007). Index methods that use GIS-based models to classify and integrate different parameters (e.g., geology, drainage, soil texture, terrain slope, land cover, and lineament/fracture/fault) have helped estimate the spatial distribution of groundwater recharge (Rwanga et al. 2017). The GIS-based index is a simplified representation of the phenomenon that uses spatial data to build a model (Jasrotia et al., 2007). The GIS approach became a widespread method to estimate groundwater recharge as it simplifies reality and extrapolates data to other areas, increasing the understanding of the system (Boumaiza et al. 2022).

The GIS-based index model technique for water balance uses spatial inputs like land use, slope, and soil type. Each parameter may have different weights according to its infiltration features (Dripps & Bradbury, 2007). Depending on the purpose and hydrological characteristics of the area, the parameters used can be subjective. Many researchers use different standards to delineate the extent of potential recharge areas. Due to the inherent uncertainty of subjective selection, comparing the results of recharge estimation using other methods is recommendable (Galvão et al., 2018).

Determining the sources of groundwater recharge is essential for effectively groundwater resource management (Yeh et al., 2014; Conicelli et al., 2021). The stable isotopes of water ($\delta^{18}O$ and δ^2H) are widely used as natural tracers to investigate hydrological processes and conceptualize groundwater recharge models (Gat, 1996; Clark & Fritz, 1997). Comparison of the isotopic composition of $\delta^{18}O$ and δ^2H from precipitation and groundwater provides a tool for evaluating the recharge mechanism (Blasch & Bryson, 2007; Heilweil et al., 2009).

The analysis of the distribution of groundwater isotopes can provide valuable information about the relative age and origin of water, identify mixtures between different water sources, and define environmental conditions during recharge, which affect water throughout the hydrological cycle (Brkić et al., 2016). Additionally, the isotopic signature, which is the stable isotope concentration distribution in groundwater, remains stable unless it is diluted or mixed with water of a different isotopic composition (Liu et al., 2019). Therefore, the spatial and temporal analysis of the isotopic signatures of precipitation, surface water, and groundwater is crucial for determining recharge zones and groundwater transit. This information is vital for understanding the hydrological processes of basins and developing conceptual hydrological models (Yin et al., 2011).

In southeastern Ecuador, the Zamora River Basin (ZRB) extends from the upper part of the Andes Mountains to the Amazon plain and the Condor Mountains. The basin has a low population density but undergoes high levels of anthropic pressure. The mining potential of the Condor Mountains in the ZRB has allowed the establishment of many copper and gold mines (Melo et al., 2013; van Teijlingen & Hogenboom, 2016). Mining activity has been the mainstay of economic activity in the region for decades affecting relatively tiny areas but could significantly impact the environment. According to some recent studies, the water quality in the basin has been affected (Villa-Achupallas et al., 2018; Mora et al., 2018, 2019).

The current growth of urban areas and the expansion of agricultural and livestock frontiers have increased deforestation processes in the basin (Torracchi, 2015). The large number of water resources required by mining, agriculture, and livestock, put at risk the supply of water available for consumption by the inhabitants of the ZRB (Mora et al., 2018). An essential part of the basin's drinking water endowment is groundwater, especially spring water (Avcı & Fernández-Salvador, 2016). Identifying recharge zones and estimating recharge values to protect water resources from anthropogenic activities, such as pollution and land-use practices that could affect the quality and quantity of clean water for consumption, is crucial (Hirata et al., 2015; Pileggi et al., 2021).

The objective of this paper is to estimate the recharge of groundwater in the Zamora River Basin (ZRB) using a distributed water balance model in GIS and to develop a conceptual hydrological model for the region employing stable isotopes ($\delta^{18}O$ and $\delta^{2}H$). This study presents an initial exploration of the evolutionary process of groundwater in the ZRB, combining two approaches: spatially distributed water balance model that uses GIS data, such as soil type, land use, and slope, and the Thornthwaite & Mather (1955) method to estimate recharge; and the use of stable isotopes to develop a conceptual hydrological model of the basin. This combined approach can serve as a useful starting point for further investigations that employ direct measurement methods.

2. Site description

The Zamora River Basin (ZRB) is located in the southern part of the Ecuadorian Amazon, covering an area of 11.369 km^2 and stretching for a length of 261 km (Fig. 1). The elevation of the ZRB decreases from 4088 to 302 meters above sea level (m.a.s.l.). The basin is limited to the east by the Condor Mountains and to the west by the Andes Mountains. The altitudinal gradient of the ZRB has a strong influence on the climate of the basin. The different climatic levels of the basin range from cold temperatures of the paramo regions in the higher areas, through the humid mesothermal on the eastern slope of the Andes Mountains, to the humid Tropical in the Amazon plain. The mean temperature varies from 6°C to 25°C depending on the altitudinal gradient, with the coldest months being June to August and the warmest months being October to December. The regional variations between the cold and hot seasons are around 1.5°C to 2.5°C and depend on the altitudinal gradient.

Precipitation in Ecuador is influenced by two primary air masses: the first originates from the Atlantic and mainly arrives from the Amazon Basin, while the second originates from the Pacific. The isotopic patterns of precipitation in Ecuador are unique, resulting in three distinct regions: the Amazon, Andean, and Pacific domains (Garcia et al., 1998). In the Pacific domain, the mean $\delta^{18}O$ values range from approximately − 2‰ in the southern part to -11‰ at altitudes above 3000 m.a.s.l. The Andean domain, located between 2500 and 3200 m.a.s.l., has an annual weighted mean $\delta^{18}O$ value ranging from − 9‰ to -11‰. The Amazon domain has annual weighted mean $\delta^{18}O$ values ranging from − 6‰ to -1‰ (Garcia et al., 1998). Due to the basin's location, the Andean and Amazonian domains may be the primary sources of groundwater recharge in the basin.

Precipitation in the Andes Mountains to the west has an average of 1380 mm/yr. The rainiest months are from February to April, while the driest months are from July to September. Instead, the easternmost area, influenced by the Condor Mountains and the Cutucú Mountains, has an average annual rainfall of 1970 mm/yr. The highest rainfall occurs from March to June, while the lowest occurs from November to February (Mora et al., 2018).

The main geological units of the basin are as follow: in the western part, there is an extensive area covered by metamorphic rocks and the Zamora Series, in addition to the Sacapalca Formation, the Tarqui Formation, and the San Lucas Batholith. Furthermore, the Zamora Batholith and the Hollin Formation cover most of the central and eastern zone, along with the Misahualli Formation to a lesser extent. The northernmost sections have the Chapiza Formation, the Napo Formation, the Santiago Formation, and the Margajitas Group (Fig. 1), according to the geospatial information provided by Ministerio de Agricultura y Ganderia.

3. Materials and methods

The research was divided into two parts: 1) estimation of groundwater recharge using a GIS-based index model, and 2) development of a groundwater recharge conceptual model using stable isotopes.

3.1. Groundwater recharge estimation using GIS-based index model

The GIS-based index method for distributed recharge integrates the water balance, adapted from Galvão et al. (2018). The first phase involved building a surface runoff map by overlaying maps of land cover, soil, and terrain slope, classified by their permeability capacities. In the second phase, the water balance method adapted from Thornthwaite & Mather (1955) was used to estimate groundwater recharge values for different water percolation scenarios. Finally, in the third phase, the water percolation flow values were used to develop the map of the groundwater recharge zone. A schematic representation and a detailed explanation of the adaptation of the Galvão et al. (2018) method are presented in Fig. 2.

3.2. Estimating runoff classes spatially by index method (Phase 1)

3.2.1. Soil permeability map

The layer of soil taxonomic classification for the Zamora Basin comes from the Geopedological map of continental Ecuador of Ministerio de Agricultura y Ganadería and contains geo-pedological and soil information updated to 2020 (Ministerio de Agricultura y Ganadería, 2019). This layer characterizes the area in ten different taxonomic types of soils: alfisols, andisols, entisols, histosols, inceptisols, mollisols, ultisols, vertisols (Fig. 3a). Additionally, this GIS information found two classes called “not applicable” and “miscellaneous lands”, defined as populated areas, bodies of water, wastelands (uncultivated land), anthropic infrastructure, and lands that are not considered land units or taxonomic units.

The reclassification of soil was determined based on the characteristic percentages of clay, sand, or silt in each taxonomic class. Soils were classified as sandy when they contained more than 72% sand, silty when the silt composition exceeded 50%, and clayey when the clay composition was greater than 40%. These values were established by the Ministry of Agriculture and Livestock (2020a). Based on these considerations, the new map of soil permeability was reclassified into two classes: 1) silty, representing low permeability or high runoff; and 2) clayey, representing almost no permeability and high runoff (as shown in Fig. 3b).

3.2.2. Land cover infiltration capacity map

The land-use layer was developed by the Ecuador Productive Systems 1:25,000 of the Ministerio de Agricultura y Ganadería (AGAP). This layer contains updated land-use information as of 2020 (Ministerio de Agricultura y Ganadería, 2020b). The classification conducted in 2020 identified twelve distinct land-use types in the area, including agricultural mosaic, anthropic infrastructure, crops, forest plantation, herbaceous vegetation, native forest, paramo (high-altitude moorland), pastureland, populated area, shrubby vegetation, wasteland, and water bodies (excluded from the analysis) (Fig. 3c). These land-use types were reclassified in two classes based on their infiltration rates to develop an infiltration capacity map: 1) forest and paramo (high permeability or low runoff); and 2) anthropic structures, crops, and pastures (low permeability or high runoff). The forest and paramo soil permeability class grouped native forest, forest plantations, shrubby vegetation, and paramo. The anthropic structures, crops, and pastures soil permeability class were grouped into the remaining seven categories (Fig. 3d).

3.2.3. Terrain slope map

The terrain slope in percentage comes from processing a DEM acquired from SIG Tierras elaborated by the MAGAP. The DEM pixel resolution is 3x3 m (Fig. 3e). Three slope intervals were defined, according to the ASCE-American Society of Civil Engineers (1969): < 2% (low slopes); 2–7% (moderate slopes); and > 7% (high slopes) (Fig. 3f).

3.2.4. Final surface runoff map

The three shapefiles: soil permeability, land cover infiltration capacity, and terrain slope (Fig. 3), were georeferenced in a GIS database in QGIS 3.10.2. The shapefiles were then converted to a 3x3 m pixel raster format (matching the DEM resolution) and then integrated into the QGIS raster calculator using the formula to calculate the runoff coefficient (Table 1). The surface runoff was estimated using twelve surface runoff classes (Table 1). The coordinate system used was UTM projection, Zone 17S, datum WGS 1984, with units in meters (Fig. 4).

Table 1
Runoff classes and their values of C in the study area. The lower the runoff coefficient, the higher the permeability capacity; the higher the runoff coefficient, the lower the permeability capacity. The values of C, C_1', C_2' and C_3' according to the Galvão et al. (2018) method.

Runoff Classes	Soil Permeability	Land Cover Infiltration Capacity	Terrain Slope (%)		Runoff Coefficient
	C'_1	C'_2	C'_3	$C = 1 - (C'_1 + C_2 + C'_3)$	C
Class 1	Silty	Forest and Paramo	< 2	1 - (0.2 + 0.2 + 0.3)	0.3
Class 2			2–7	1 - (0.2 + 0.2 + 0.2)	0.4
Class 3			> 7	1 - (0.2 + 0.2 + 0.1)	0.5
Class 4		Anthropic structures, crops and pastures	< 2	1 - (0.2 + 0.1 + 0.3)	0.4
Class 5			2–7	1 - (0.2 + 0.1 + 0.2)	0.5
Class 6			> 7	1 - (0.2 + 0.1 + 0.1)	0.6
Class 7	Clayey	Forest and Paramo	< 2	1 - (0.1 + 0.2 + 0.3)	0.4
Class 8			2–7	1 - (0.1 + 0.2 + 0.2)	0.5
Class 9			> 7	1 - (0.1 + 0.2 + 0.1)	0.6
Class 10		Anthropic structures, crops and pastures	< 2	1 - (0.1 + 0.1 + 0.3)	0.5
Class 11			2–7	1 - (0.1 + 0.1 + 0.2)	0.6
Class 12			> 7	1 - (0.1 + 0.1 + 0.1)	0.7

3.3. Water balance for each class of the surface runoff map (Phase 2)

The water balance was estimated using daily mean temperature and precipitation data obtained from meteorological stations of the Instituto Nacional de Meteorologia e Hidrologia (INAMHI), Ecuador's meteorological service. Despite the basin's vast area (less than 11,000 km^2), only five stations (shown in Fig. 5) have recorded historical precipitation and temperature data for the ZRB. Data reanalysis was made to compensate for the lack of historical data and complement the spatial analysis of precipitation and temperature. The climate reanalysis data were calibrated and used as a proxy to reproduce local climate variability. Data from ECMWF Copernicus Climate Change Service (2017) were used to estimate surface air temperature (2 m temperature) and from TRMM Tropical Rainfall Measuring Mission (2011) for precipitation data. Five points were defined to spatially locate the reanalysis results; the location of these points depended on spatial parameters of distance and representativeness (Fig. 5). The reanalysis data were validated using the method proposed by Erazo et al. (2018) for precipitation and the methods proposed by de Oliveira Aparecido et al. (2020) for temperature.

Due to the extension of the basin, the water balance was estimated across six distinct precipitation blocks. The water balance analysis was conducted for each of the twelve classes of surface runoff within each of these six blocks, utilizing the methodology outlined by Pereira (2005), covering the period from 1998 to 2019. Temperature and precipitation values for each block were determined based on data averages obtained from the INAMHI climatological stations and reanalysis result points, as outlined in Table 2.

Table 2
Climatological data used for water balance in each block from 1998 to 2019. The monthly values for each precipitation block are the average data from meteorological stations and the reanalysis result points.

Mean precipitation 1998–2019 (mm)												
	Jan	**Feb**	**Mar**	**Apr**	**May**	**Jun**	**Jul**	**Aug**	**Sep**	**Oct**	**Nov**	**Dec**
Block 1	83	96	111	76	68	60	54	38	45	61	58	67
Block 2	98	130	145	98	68	58	52	40	38	80	73	95
Block 3	118	132	175	143	115	100	66	54	71	74	83	94
Block 4	143	161	197	179	131	103	88	79	87	101	114	131
Block 5	142	145	190	193	186	185	144	106	121	132	127	135
Block 6	168	146	220	217	207	237	176	142	150	145	149	136
Mean temperature 1998–2019 (°C)												
	Jan	**Feb**	**Mar**	**Apr**	**May**	**Jun**	**Jul**	**Aug**	**Sep**	**Oct**	**Nov**	**Dec**
Block 1	14.8	14.8	14.8	15.0	14.9	14.2	13.7	14.3	15.1	14.9	14.6	14.7
Block 2	16.2	16.3	16.5	16.6	16.4	15.7	15.2	15.6	16.2	16.6	16.7	16.5
Block 3	19.7	19.8	20.0	20.1	19.9	19.2	18.7	19.1	19.7	20.1	20.2	20.0
Block 4	22.8	22.8	22.8	22.6	22.2	21.2	20.7	21.1	22.0	22.8	23.2	23.1
Block 5	23.6	23.4	23.5	23.4	23.0	22.1	21.6	21.9	22.6	23.5	24.0	23.8
Block 6	18.8	18.8	18.9	18.8	18.5	17.7	17.3	17.9	18.5	18.8	18.9	18.7

3.4. Groundwater Recharge Map of Zamora River Basin ZRB (Phase 3)

Phases one and two were used to estimate the areas of different recharge rates in the ZRB. The final surface runoff map (Fig. 4) shows the twelve soil classes based on their potential recharge capacity. This map provides information on the annual recharge ratio obtained through the water balances for the flow of one of the six precipitation blocks, and allows the spatial distribution of the groundwater recharge for the entire basin to be obtained. The spatial distribution of recharge in four regions was then categorized according to their annual recharge capacity (Table 3) to create the final ZRB groundwater recharge map (Fig. 5).

Table 3
Classification of groundwater recharge zones for the Zamora River Basin (ZRB)

Recharge Zone		**Recharge Ratio**
Zone 1	High recharge values	> 100 mm/yr
Zone 2	Moderate recharge values	50–100 mm/yr
Zone 4	Low recharge values	25–50 mm/yr
Zone 5	Incipient recharge values	< 25 mm/yr

3.4.1. Recharge Conceptual Model using stable isotopes $\delta^{18}O$ and $\delta^{2}H$

The data from stable isotopes $\delta^{18}O$ and $\delta^{2}H$ came from the ECU7007 project "Strengthening the Management and Water Quality Control of the Zamora River Basin through the Application of Isotope Techniques" developed by the Ministry of Environment, Water and Ecological Transition with the support of the International Atomic Energy Agency. The data include two water stable isotopes sampling campaigns. The campaigns were carried out in January (for wet season) and September (for dry season) 2018. The sampling sites were: five precipitation points, eighteen superficial points, and ten spring water points (Fig. 6). For this study, we only had access to isotopic information from the first campaign.

4. Results and discussion

4.1. Groundwater recharge estimation

4.1.1. Estimating runoff classes spatially by the index method

Clayey soils constitute most of the basin soil, mainly inceptisols covering ~ 75% of the ZRB area. However, silty soils are distributed in patches around the entire basin. There are no sandy soils within the basin (Fig. 3b). The predominant presence of clay soils (~ 82%) implies a waterproofing effect that generates high runoff and hinders high groundwater recharge rates in the ZRB (Koerner & Daniel, 1997).

Most of the ZRB area is covered by native forest (~ 70%), followed by grasslands (14%) and agricultural mosaics (4.8%) concentrated around populated sites and river stretches. The infiltration capacity map (Fig. 3d) reveals that reclassification locates most of the basin as a class of forest and paramo associated with high potential permeability (Terada et al., 2022). The westernmost part of the ZRB concentrates places of high groundwater recharge, such as paramos. The other classifications, such as forest plantations and shrub vegetation, each occupy less than 0.2% of the basin. The class anthropic structures, crops, and pastures are distributed throughout the watershed, especially the plains covered by pastureland near rivers and populated areas.

The watershed has a maximum altitude of 4088 m.a.s.l. to a minimum of 302 m.a.s.l. (Fig. 3e). That is an altitude variation of almost 3,800 m and an average slope of 1.6%. Flat areas, < 2%, cover approximately 69.23% of the ZRB, followed by areas with moderate slopes, 2–7%, representing 30.7%, and a practically imperceptible number of sites with high slopes > 7%, almost 0.07%. To explain the low slopes in a large altitudinal gradient, the hypsometric curve of the basin was revised, indicating that it has reached equilibrium and is in the maturity phase, which did not explain the observation of low slopes in the ZRB. Slopes may decrease as resolution increases. So, it was attributed to low slopes that may be biased given the resolution of the digital elevation model DEM (Chang & Tsai, 1991).

4.1.2. Water balance estimations for each class of the surface runoff map

The description of groundwater recharge in ZRB is in Fig. 7, and the area distributions are shown in Fig. 8. The integration of the twelve surface runoff classes with the six precipitation blocks generated seventy-two recharge areas. The results (Fig. 7) indicated that, for precipitation block one, the recharge values for runoff classes one and two are between incipient (9 mm/yr) and low (30 mm/yr). The remaining the runoff classes had incipient recharge values (< 9 mm/yr). In precipitation block one, clay soils (Fig. 3b) and moderate annual precipitation of 818.7 mm/yr (Table 2) did not provide the necessary conditions for significant groundwater recharge.

Precipitation block two (Fig. 5) has an annual rainfall of 976 mm/yr and recorded recharge values between 9 and 80 mm/yr for all classes, except for runoff, and classes six, eleven, and twelve. Runoff class one had a moderate discharge rate, while runoff classes two, four, and seven had low recharge rates. The rest of the runoff classes had incipient recharge values.

Precipitation blocks three and four (Fig. 5) had an annual rainfall of 1226 and 1514 mm/yr, respectively (Table 2), and recorded maximum recharge values of 105 and 106 mm/yr, respectively, for runoff class one. Both precipitation blocks registered low recharge values (47 mm/yr) for runoff classes two, four, and seven and incipient (2 and 11 mm/yr) for runoff classes three, five, eight, and ten. No recharge was registered for classes six, nine, eleven, and twelve. The groundwater recharge in precipitation blocks three and four has similar values in all runoff classes, even considering a precipitation difference of 288 mm/yr. The differentiating factor between these precipitation blocks was the temperature, 19.7°C for precipitation block three and 22.3°C for block four. In the Thornthwaite & Mather (1955) method, evapotranspiration is directly linked to temperature. The temperature difference of 2.6°C between blocks three and four was reflected in the evapotranspiration values. The higher temperature of block four increased the evapotranspiration values and canceled the effect of the additional precipitation that this block has.

Precipitation blocks five and six had an annual rainfall of 1805 and 2092 mm/yr (Fig. 5, Table 2) and maximum recharge values of 184 and 642 mm/yr, respectively. Runoff class one has the highest recharge values. Precipitation block five has high recharge values (85 mm/yr) for runoff classes two, four, and seven; it has incipient recharge (11 mm/yr) for classes three, five, eight, and ten. Runoff classes six, nine, and eleven did not have a recharge. Precipitation block six had high recharge values (642, 433, and 223 mm/yr) for runoff classes one, two, three, four, five, seven, eight, and ten, high recharge values (55 mm/yr) for classes six, nine and eleven and class twelve has no recharge.

The recharge values of precipitation block six were very different from those of the rest of the precipitation blocks. The high recharge values for precipitation block six were related to the fact that it has an average annual rainfall of 2,092 mm/yr (Table 2), the highest in the ZRB. In addition, the

temperature of this block has an annual average of 18.5°C; this is on average 4°C colder than that of blocks four and five. Lower evapotranspiration values implied higher percolation values (Koerner & Daniel, 1997). The high precipitation and low evapotranspiration (due to the low temperature) caused the unusual and high recharge rate for this precipitation block.

In the Galvão et al. (2018) method, soil composition (sandy, silty, and clayey) had the most significant weight in determining soil permeability. The soils in the ZRB were composed only of loamy and clayey soils with low permeability. However, the area has favorable characteristics for recharge, such as slopes < 7% and native forest cover (Fig. 3), which increase the probability of groundwater recharge. It is also important to highlight that, despite the importance of soil features in recharge processes (Fig. 4), annual precipitation was the most significant individual driver of groundwater recharge, as indicated by (Conicelli et al., 2021).

4.1.3. Groundwater Recharge Map of Zamora River Basin (ZRB)

Zone 1 (blue, Fig. 8) represents 18.22% of the basin registered high recharge rates, with values greater than 100 mm/yr. It includes runoff class one of precipitation blocks three, four, and five and runoff classes one, two, three, four, five, seven, eight, and ten of precipitation block six. This area is mainly located at the mouth of the basin, in the northern part of the ZRB, which is precipitation block six. It is distributed in patches in the central and northern part of precipitation blocks four and five and small areas in the center precipitation block three. It occurs when C = 0.3 in precipitation blocks three, four, and five and when C = 0.4–0.5 (Table 1) in precipitation block six.

Zone 2 (green, Fig. 8) represents 30.93% of the basin and registered moderate recharge rates with values between 50 and 100 mm/yr. It includes runoff class one of precipitation block two, classes two, four, and seven of precipitation block five, and runoff classes six, nine, and eleven of precipitation block six. It occurs when C = 0.3 in precipitation block two, when C = 0.4 in precipitation block five, and when C = 0.6 in precipitation block six (Table 1). This zone can be seen as small scattered patches in the northwestern part of precipitation block six, covering most of the whole of precipitation block five and scattered zones in the north and south part of precipitation block two.

Zone 3 (yellow, Fig. 8) represents 18.82% of the basin and registered low recharge rates with values from 25 to 50 mm/yr. It includes runoff class one of precipitation block one and runoff classes two, four, and seven of precipitation blocks two, three, and four. It occurs when C = 0.3 in precipitation block one and when C = 0.4 in precipitation blocks two, three, and four (Table 1). This zone can be identified as several small zones scattered in precipitation blocks one, two, three, and four of the ZRB.

Zone 4 (orange, Fig. 8) represents 32.04% of the basin registering incipient recharge rates, with values lower than 25 mm/yr. It includes the remaining runoff classes of all blocks. It occurs when C = 0.7 in all precipitation blocks, when C = 0.5–0.6 in precipitation blocks one to four and when C = 0.4 in precipitation block one (Table 1). This area is distributed as scattered patches around the entire basin, except in precipitation block six.

It is essential to consider that although some areas have low recharge rates and high surface runoff, they are close to areas of high and moderate recharge rates. Therefore, the water drained from areas of high recharge located at a higher elevation can reach areas with low percolation (Galvão et al., 2018). Despite the ZRB being covered with clayey and silty soil, the low slopes, the coverage of native forest, and especially the high precipitation values for the entire basin make the ZRB, as a whole, a vital recharge area for the Amazon foothills.

The ultimate goal of GIS-based groundwater recharge analysis is not to present a definitive recharge map of the ZRB but to provide a simplified representation of reality to help predict the impacts of anthropogenic activity in the basin. It mainly considers land-use change processes and the dispersion of pollutants from mining that can affect the supply of surface and groundwater available to people living within the ZRB.

The most important groundwater recharge zones in the basin are located further east, next to the Condor Mountains. Some of Ecuador's large-scale mining projects are located in the Condor Mountains area. Although the effects or influences of mining on the groundwater regime are not yet well understood, the location of these mining projects above these potentially important groundwater recharge zones poses a serious contamination hazard. Activities such as the disposal of wastewater from plants, pumping water from the mine, or washing waste and tailings dumps are potential sources of heavy metal contamination for groundwater (Raghavendra & Deka, 2015).

4.2. Recharge conceptual model using stable isotopes $\delta^{18}O$ and $\delta^{2}H$

The stable isotope data for precipitation samples from ZRB ranged from − 2.89‰ to − 6.53‰ for $\delta^{18}O$ and from − 9.41‰ to − 40.14‰ for $\delta^{2}H$. The deuterium excess was between 10.53‰ and 13.71‰ (Table 4). The Local Meteorological Water Line (LMWL) is $\delta^{2}H = 8.32\delta^{18}O + 13.50$ (Fig. 9), which was plotted above the GMWL ($\delta^{2}H = 8\delta^{18}O + 10$) (Fig. 9). The equation that describes the LMWL is similar to those described by Garcia et al. (1998) in Méndez, 30 km north of ZRB, whose equation is $\delta^{2}H = 8.51\delta^{18}O + 13.53$, and is similar to that described by Jiménez et al. (2022) at the Ikiam meteorological station, 225 km north of ZRB, whose equation is $\delta^{2}H = 8.4\delta^{18}O + 15.3$). In Jiménez et al. (2022), isotopic values and back-trajectory analyses using the HYSPLIT model revealed that the isotopic signature was affected by the moisture source effect associated with upstream rainout. The moisture flux was primarily from an east-to-northeast direction, originating from the Atlantic Ocean and passing through the Amazon Basin. The d-excess values of rainfall and the LMWLs indicated an influence of the high evapotranspiration rate of the Amazon region on the isotopic composition of local precipitation.

Comparison of the regression line of the ZRB with the LMWLs of Méndez and Ikiam stations showed that these three LMWLs are not statistically different (R2 = 0.99; p-value < 0.05 for both cases). The similarity of the isotopic composition of the precipitation from the Napo province (Ikiam station location) to Mendez and ZRB may indicate that the precipitation in this entire area of the Ecuadorian Amazon has the same origin. For the ZRB's LMWL, only stable isotope data from the rainy season of the basin was used. Therefore, the equation that describes the LMWL may vary slightly with the data from the dry season.

Fractionation is the change in the isotopic composition of precipitation, influenced by the origin of air masses, elevation, continentality, and latitude. The isotopic composition alteration is also influenced by the climatic patterns of unique precipitation events (Crawford et al., 2013). Continentality is one factor that explains the substantial depletion of isotopes as an air mass moves inland, causing precipitation to become more negative with a deficit of heavier isotopes (Dansgaard, 1964). However, for the ZRB, the altitudinal effect is the most influential factor that favors the depletion of isotopes in precipitation. However, for the ZRB, the altitudinal effect is the most influential factor that favors the depletion of isotopes in precipitation. As the humidity from the Amazon plain passes over an orographic barrier, such as the Andes Mountains, it is forced upwards, and the temperature reduces, which favors preferential rainfall and the depletion of heavy isotopes (Dansgaard, 1964; Cabrera et al., 2021; Jiménez et al., 2022; Calero et al., 2022). The altitudinal effect of $\delta^{18}O$ in the basin is evident; at a lower altitude, there is an enrichment of $\delta^{18}O$ in the water samples and vice versa (Cabrera et al., 2021; Jiménez et al., 2022; Calero et al., 2022). Although for point P4, there is an exaggerated enrichment due to other factors, such as water recycling processes. The average of the altitudinal isotopic gradient of the ZRB for every 100 m is -0.17, and this result is consistent with the altitude isotope gradient of Garcia et al. (1998) and Maldonado-Astudillo et al. (1995).

Table 4
Isotopic composition in precipitation samples of ECU7007 project.

ID	Elevation	Date	$\delta^{18}O$ (‰)	$\delta^{2}H$ (‰)	d-excess (‰)
P1	2525	1/20/2018	-6.53	-40.14	12.10
P2	2160	11/28/2018	-6.41	-39.84	11.44
P3	1835	1/21/2018	-5.57	-33.14	11.42
P4	837	1/20/2018	-2.89	-9.41	13.71
P5	766	1/19/2018	-4.14	-22.59	10.53

The LMWL constructed from the precipitation samples (Fig. 9) shows that there are two types of precipitation samples: the Andean group (P1, P2, P3, in Fig. 6A), which records the most impoverished $\delta^{18}O$ values, and the Amazon group (P4 and P5 in Fig. 6A), which has the most enriched $\delta^{18}O$ values. Furthermore, it is noticeable that the isotopic signature of the surface and spring water samples is closer to the Andean group (Fig. 9). This depletion of $\delta^{18}O$ in the Andean group is mainly due to the altitudinal effect; the samples of this group register altitudes higher than 1800 m.a.s.l., and those of the Amazon group have elevations lower than 850 m.a.s.l.

Dansgaard (1964) established deuterium as an indicator of the source region of precipitation and the variations within the source area. The trajectories of air masses and areas of moisture sources can be traced with deuterium to improve the understanding of regional climate systems (Jansson et al., 2007). Deuterium changes seasonally with warm-dry sources showing high values and cold-humid sources showing low values. The average d-excess detected in the samples (11.86‰) and values ranging from 10.51‰ to 13.73‰ (Table 5) indicate the source of moisture may come from the Amazon plain (Jiménez et al., 2022). According to Salati et al. (1979), the deuterium of the air masses that cross the Amazon remains in a range of 9.80‰ to 14.60‰, confirming the results.

However, point P4 (Fig. 6A) presents a value > 13‰, which is unusually higher than the remaining sample points of the Andean Group, suggesting recycling processes within the basin. The d-excess for all surface water samples is also > 13‰, indicating that the surface water that runs through the watershed has undergone recycling processes. The documentation of recycling processes exists for the entire Amazon basin (Salati et al., 1979; Victoria et al., 1991). Since the ZRB is limited to the west by the Andes and the east by the Condor Mountains (Fig. 10), a recirculation process may be a persistent feature. For most samples, the d-excess of spring water is between 8‰ and 12‰, typical of meteoric processes. However, there are three spring water points (G1, G3, G6 in Fig. 6C) with a d-excess > 13‰. The groundwater recharge processes in the ZRB are governed mainly by the regional precipitation of the Amazon basin that comes from the Atlantic Ocean and crosses the entire Amazon until it collides with the Andes Mountains (Fig. 10) (Victoria et al., 1991; Souza et al. 2015).

The isotopic signature of the spring water samples is close to the precipitation samples of the Andean Group (Table 5) (Fig. 9). Previous research has established that the source of the precipitation of the Andean Group is the moisture coming from the Amazonian plain, likely including recycling processes within the ZRB (Fig. 10) (Cabrera et al., 2021; Jiménez et al., 2022; Calero et al., 2022). It has been established that the primary source of groundwater recharge of the ZRB is the precipitation from the Amazon basin and recycling processes within the basin. However, while the stable isotope analysis may suggest that there are no direct inputs of surface water to the groundwater samples studied, it is important to note that this conclusion is based on a limited data set and mat not apply to all groundwater sources in the region. Further studies are needed to fully understand the relationship between surface water and groundwater in the area. Additional isotopic analysis, hydrological modeling, and field observations could provide a more comprehensive understanding of the sources of recharge for groundwater in the ZRB. Therefore, although GIS and stable isotope analysis are useful tools for understanding the origins of groundwater, further studies are required to characterize the groundwater recharge in the ZRB.

Table 5
Statistical summary of isotopic table compositions in precipitation, superficial, and spring water samples in Zamora River Basin (ZRB).

Precipitation (n = 5)	δ^2H (‰)	$\delta^{18}O$ (‰)	d-excess (‰)
Min	-40.14	-6.53	10.51
Max	-9.41	-2.89	13.73
Mean	-29.02	-5.11	11.86
Std	13.07	1.57	1.20
Superficial water (n = 18)			
Min	-53.88	-8.57	13.21
Max	-34.06	-5.99	14.77
Mean	-44.35	-7.30	14.05
Std	5.58	0.72	0.50
Springwater (n = 10)			
Min	-47.52	-7.58	10.87
Max	-36.25	-5.93	13.60
Mean	-41.08	-6.65	12.12
Std	3.25	0.49	0.95

5. Conclusions

This study aims to establish the relationship between the factors influencing groundwater recharge and a GIS-based distributed water balance model to produce a groundwater recharge potential map and apply it to a large-scale basin, such as the ZRB. The applied method is a helpful tool for estimating groundwater recharge, especially for areas with little or no hydrogeological information available.

The soil of the ZRB is mainly waterproof (high clay content); however, because of the low slopes (< 7%) and native forest cover enhance groundwater recharge. Despite the importance of soil type, precipitation is the single most significant driver of groundwater recharge in the ZRB. High precipitation rates cover the basin with high (18.22%) and moderate (30.93%) recharge zones.

The most effective groundwater recharge potential zone is downstream, located at the basin outlet in block six, where the abundant precipitation allows high groundwater recharge rates reaching more than 640 mm/yr. The fact that the mining activity is in this vital groundwater recharge area poses a constant danger to the water quality of the Amazon basin. Some of the most important mining projects in Ecuador operate in this area, located in the northern part of the Condor Mountains. The pollutants from mining could be transferred in groundwater from the ZRB to the following basins, such as the Santiago River basin and the Peruvian territory.

The stable isotope data ($\delta^{18}O$ and δ^2H) indicate that most of the rainfall precipitating in the basin comes from moisture transported from the Amazon plain. There are also recycling processes in the ZRB. They also indicate that the principal groundwater recharge comes from precipitations from Amazon humidity and recirculation processes within the ZRB. This information is consistent with other stable isotope studies conducted in the Amazon region of Ecuador. However, a broader sampling of the isotopic composition is required temporally and spatially to confirm the model.

Declarations

Statements & Declarations

Funding

The authors declare that no funds, grants, or other support were received during the preparation of this manuscript.

Competing Interests

The authors have no relevant financial or non-financial interests to disclose.

Author Contributions

All authors contributed to the study conception and design. Material preparation, data collection and analysis were performed by Alexander Gualli, Bruno Conicelli and Paulo Galvão. The first draft of the manuscript was written by Alexander Gualli and all authors commented on previous versions of the manuscript. All authors read and approved the final manuscript.

Acknowledgments

Thanks to the Ministry of Agriculture of Livestock of Ecuador for providing the geospatial information for this study, to the Ministry of Environment, Water and Ecological Transition of Ecuador for sharing the isotopic information of the ECU7007 project and National Institute of Hydrology and Meteorology for the meteorological data. There are no conflicts of interest to declare.

References

1. Allison, G. B. (1988). A Review of Some of the Physical, Chemical and Isotopic Techniques Available for Estimating Groundwater Recharge. Estimation of Natural Groundwater Recharge, 49–72. https://doi.org/10.1007/978-94-015-7780-9_4
2. Andreo, B., Vías, J., Durán, J. J., Jiménez, P., López-Geta, J. A., & Carrasco, F. (2008). Methodology for groundwater recharge assessment in carbonate aquifers: Application to pilot sites in southern Spain. Hydrogeology Journal, *16*(5), 911–925. https://doi.org/10.1007/s10040-008-0274-5
3. ASCE-American Society of Civil Engineers. (1969). Effect of urban development on flood discharges. Current knowledge and future needs. Journal of the Hydraulics Division, *95*(HY1), 287–309.
4. Avcı, D., & Fernández-Salvador, C. (2016). Territorial dynamics and local resistance: Two mining conflicts in Ecuador compared. Extractive Industries and Society, *3*(4), 912–921. https://doi.org/10.1016/j.exis.2016.10.007
5. Blasch, K. W., & Bryson, J. R. (2007). Distinguishing sources of ground water recharge by using δ2H and δ18O. Ground Water, *45*(3), 294–308. https://doi.org/10.1111/J.1745-6584.2006.00289.X
6. Brkić, Ž., Briški, M., & Marković, T. (2016). Use of hydrochemistry and isotopes for improving the knowledge of groundwater flow in a semiconfined aquifer system of the Eastern Slavonia (Croatia). Catena, *142*, 153–165. https://doi.org/10.1016/j.catena.2016.03.010
7. Cabrera, M., Moulatlet, G. M., Valencia, B. G., Maisincho, L., Rodríguez-Barroso, R., Albendín, G., Sakali, A., Lucas-Solis, O., Conicelli, B., & Capparelli, M. V. (2021). Microplastics in a tropical Andean Glacier: A transportation process across the Amazon basin? Science of The Total Environment, *805*, 150334. https://doi.org/10.1016/j.scitotenv.2021.150334
8. Calero, J. L., Conicelli, B., & Valencia, B. G. (2022). Determination of an age model based on the analysis of the δ 18O cyclicity in a tropical glacier. *Journal of South American Earth Sciences*, *116*. https://doi.org/10.1016/j.jsames.2022.103808
9. Chang, K. T., & Tsai, B. W. (1991). The effect of dem resolution on slope and aspect mapping. Cartography and Geographic Information Systems, *18*(1), 69–77. https://doi.org/10.1559/152304091783805626
10. Conicelli, B., Hirata, R., Galvão, P., Bernardino, M., Simonato, M., Abreu, M. C., Aranda, N., & Terada, R. (2021). Determining groundwater availability and aquifer recharge using GIS in a highly urbanized watershed. *Journal of South American Earth Sciences*, *106*. https://doi.org/10.1016/j.jsames.2020.103093
11. Conicelli, B., Hirata, R., Galvão, P., Aranda, N., Terada, R,. Gutiérrez, O.J.G. (2021). Groundwater governance: The illegality of exploitation and ways to minimize the problem. ANAIS DA ACADEMIA BRASILEIRA DE CIENCIAS, v. 93, p. e20200623. https://doi.org/10.1590/0001-3765202120200623
12. Copernicus Climate Change Service (C3S). (2017). *ERA5: Fifth generation of ECMWF atmospheric reanalyses of the global climate*... Copernicus Climate Change Service Climate Data Store (CDS). https://cds.climate.copernicus.eu/cdsapp#!/home
13. Crawford, J., Hughes, C. E., & Parkes, S. D. (2013). Is the isotopic composition of event based precipitation driven by moisture source or synoptic scale weather in the Sydney Basin, Australia? Journal of Hydrology, *507*, 213–226. https://doi.org/10.1016/j.jhydrol.2013.10.031
14. Dansgaard, W. (1964). Stable isotopes in precipitation. Tellus, *16*(4), 436–468. https://doi.org/10.1111/J.2153-3490.1964.TB00181.X
15. de Oliveira Aparecido, L. E., de Souza Rolim, G., & da Silva Cabral de Moraes, J. R. (2020). Validation of ECMWF climatic data, 1979–2017, and implications for modelling water balance for tropical climates. *International Journal of Climatology*, *40*(15), 6646–6665. https://doi.org/10.1002/joc.6604
16. Dripps, W. R., & Bradbury, K. R. (2007). A simple daily soil-water balance model for estimating the spatial and temporal distribution of groundwater recharge in temperate humid areas. Hydrogeology Journal, *15*(3), 433–444. https://doi.org/10.1007/s10040-007-0160-6
17. El Khalil, H., El Hamiani, O., Bitton, G., Ouazzani, N., & Boularbah, A. (2008). Heavy metal contamination from mining sites in South Morocco: Monitoring metal content and toxicity of soil runoff and groundwater. Environmental Monitoring and Assessment, *136*(1–3), 147–160. https://doi.org/10.1007/s10661-007-9671-9
18. Erazo, Bolívar, Luc Bourrel, Frédéric Frappart, Oscar Chimborazo, David Labat, Luis Dominguez-Granda, David Matamoros, and Raul Mejia. 2018. "Validation of Satellite Estimates (Tropical Rainfall Measuring Mission, TRMM) for Rainfall Variability over the Pacific Slope and Coast of Ecuador" Water 10, no. 2: 213. https://doi.org/10.3390/w10020213
19. Fenn, D., Hanley, K., & DeGeare, T. (1975). *Use of the water-balance method for predicting leachate generation from solid-waste-disposal sites*. https://www.osti.gov/biblio/6328350
20. Freeze, R. A., & Cherry, J. A. (1979). *Groundwater*. Prentice-Hall.
21. Galvão, P., Hirata, R., & Conicelli, B. (2018). Estimating groundwater recharge using GIS-based distributed water balance model in an environmental protection area in the city of Sete Lagoas (MG), Brazil. Environmental Earth Sciences, *77*(10), 1–19. https://doi.org/10.1007/s12665-018-7579-z
22. Garcia, M., Villalba, F., Araguas Araguas, L., & Rozanski, K. (1998). The role of atmospheric circulation patterns in controlling the regional distribution of stable isotope contents in precipitation: Preliminary results from two transects in the Ecuadorian Andes. *Isotope Techniques in the Study of*

Environmental Change. Proceedings of a Symposium, Vienna, April 1997., 127–140. https://inis.iaea.org/Search/search.aspx?orig_q=RN:29044418

23. Healy, R. W., & Scanlon, B. R. (2011). Estimating groundwater recharge. In *Estimating Groundwater Recharge* (Vol. 9780521863). https://doi.org/10.1017/CBO9780511780745
24. Heilweil, V. M., Solomon, K. D., Gingerich, S. B., & Verstraeten, I. M. (2009). Oxygen, hydrogen, and helium isotopes for investigating groundwater systems of the Cape Verde Islands, West Africa. Hydrogeology Journal, *17*(5), 1157–1174. https://doi.org/10.1007/S10040-009-0434-2
25. Hendrickx, J. M. H. (1992). Groundwater Recharge. A Guide to Understanding and Estimating Natural Recharge (Volume 8, International Contributions to Hydrogeology). Journal of Environmental Quality, *21*(3), 512–512. https://doi.org/10.2134/jeq1992.00472425002100030036x
26. Hirata, R.; Conicelli, B. P. ; Pinhatti, Antonio ; Luiz, M. B. ; Porto, R. ; Ferrari, L. C. K. M. (2015). O Sistema Aquífero Guarani e a crise hídrica nas regiões de Campinas e São Paulo (sp). REVISTA USP, p. 59.v https://doi.org/10.11606/issn.2316-9036.v0i106p59-70
27. Jansson, P., Linderholm, H. W., Pettersson, R., Karlin, T., & Mörth, C. M. (2007). Assessing the possibility to couple the chemical signal in winter snow on Storglaciären, Sweden, to atmospheric climatology. Annals of Glaciology, *46*, 335–341. https://doi.org/10.3189/172756407782871459
28. Jasrotia, A. S., Kumar, R., & Saraf, A. K. (2007). Delineation of groundwater recharge sites using integrated remote sensing and GIS in Jammu district, India. International Journal of Remote Sensing, *28*(22), 5019–5036. https://doi.org/10.1080/01431160701264276
29. Jiménez-lñiguez, A., Ampuero, A., Valencia, B. G., Mayta, V. C., Cruz, F. W., Vuille, M., Novello, V. F., Misailidis Stríkis, N., Aranda, N., & Conicelli, B. (2022). Stable isotope variability of precipitation and cave drip-water at Jumandy cave, western Amazon River basin (Ecuador). *Journal of Hydrology*, *610*. https://doi.org/10.1016/j.jhydrol.2022.127848
30. Koerner, R., & Daniel, D. (1997). Final Covers for Solid Waste Landfills and Abandoned Dumps. In *Final Covers for Solid Waste Landfills and Abandoned Dumps*. https://doi.org/10.1680/fcfswlaad.9780784402610
31. Liu, F., Song, X., Zhen, P., Wang, L., & Wang, S. (2019). Insights from stable isotopes of water and hydrochemistry to the evolutionary processes of groundwater in the Subei lake basin, Ordos energy base, Northwestern China. Isotopes in Environmental and Health Studies, *55*(5), 438–458. https://doi.org/10.1080/10256016.2019.1654472
32. Maldonado-Astudillo, S., Cepeda-Tobar, H., & Araguas-Araguas, L. (1995). Hydrogeological and isotopic study of the Guayas river Delta aquifers (Ecuador); Estudio hidrogeologico e isotopico de los acuiferos del Delta del Rio Guayas. (in Spanish). International Atomic Energy Agency, *27*(6), 195–209. https://inis.iaea.org/search/search.aspx?orig_q=RN:27018956
33. Mazor, E. (2004). Chemical and Isotopic Groundwater Hydrology Third Edition. In *Applied Chemical and Isotopic Groundwater Hydrology*. https://books.google.es/books?hl=es&lr=&id=AUND-o9klhMC&oi=fnd&pg=PR3&dq=Chemical+and+isotopic+groundwater+recharge&ots=d0j7wa8kv8&sig=3F7N1r0LLiZ43ssnhmnyL9YPnnY
34. Melo, C., Mena, C. F., Arsel, M., & Pellegrini, L. (2013). The State is dead, Long Live the State: Re-inserting the State in the Gold-mining Industry in Zamora-Chinchipe, Ecuador. *CoCooN NEBE Working Paper*, 1–37. https://doi.org/10.13140/RG.2.1.3891.7603
35. Ministerio de Agricultura y Ganadería. (2019). *Mapa Geopedológico del Ecuador continental (versión editada por el Ministerio de Agricultura y Ganadería en 2019), escala 1:25.000, año 2009–2015 [Conjunto de datos]*. http://geoportal.agricultura.gob.ec/geonetwork/srv/spa/catalog.search;jsessionid=7D2B95F7009FE6AFF197413E174AD567#/metadata/0a26e971-5722-4a10-8a5e-d04298b0f017
36. Ministerio de Agricultura y Ganadería. (2020a). *Catalogo de objetos Geográficos y Productos Cartográficos agropecuarios del Ministerio de Agricultura y Ganadería*. http://geoportal.agricultura.gob.ec/pdf/catalogo_mag_vol_IV.pdf
37. Ministerio de Agricultura y Ganadería. (2020b). *Mapa de Cobertura y uso de la tierra y Sistemas productivos agropecuarios del Ecuador continental*. http://geoportal.agricultura.gob.ec/geonetwork/srv/spa/catalog.search;jsessionid=7D2B95F7009FE6AFF197413E174AD567#/metadata/4f7e118f-0439-42bf-ab62-f0e7c842a379
38. Mora, A., Jumbo-Flores, D., González-Merizalde, M., Bermeo-Flores, S. A., Alvarez-Figueroa, P., Mahlknecht, J., & Hernández-Antonio, A. (2019). Heavy Metal Enrichment Factors in Fluvial Sediments of an Amazonian Basin Impacted by Gold Mining. Bulletin of Environmental Contamination and Toxicology, *102*(2), 210–217. https://doi.org/10.1007/s00128-019-02545-w
39. Mora, A., Jumbo Flores, D., & Mahlknecht, J. (2018). Levels of MN, ZN, PB and HG in sediments of the zamora river, Ecuador. Revista Internacional de Contaminacion Ambiental, *34*, 245–249. https://www.researchgate.net/profile/Diogenes-Hernandez-3/publication/330141509_Characterizing_the_evolution_of_sediment_like_wastes_exposed_to_ambient_conditions_in_open_reservoirs/links/5c2f5b6da6fdccd6b590bf0c/Characterizing-the-evolution-of-sediment-l
40. Nolan, B. T., Healy, R. W., Taber, P. E., Perkins, K., Hitt, K. J., & Wolock, D. M. (2007). Factors influencing ground-water recharge in the eastern United States. Journal of Hydrology, *332*(1–2), 187–205. https://doi.org/10.1016/j.jhydrol.2006.06.029
41. Pereira, A. R. (2005). Simplificando o balanco hidrico de Thornthwaite and Mather. Bragantia, *64*(2), 311–313.
42. Pileggi, F., Hirata, R., Aranda, N., & Conicelli, B. (2021). Support method for interpretation of regional groundwater monitoring in urban areas. Brazilian Journal of Geology, *51*(2). https://doi.org/10.1590/2317-4889202120200053
43. Raghavendra, N. S., & Deka, P. C. (2015). Sustainable Development and Management of Groundwater Resources in Mining Affected Areas: A Review. Procedia Earth and Planetary Science, *11*, 598–604. https://doi.org/10.1016/j.proeps.2015.06.061
44. Rwanga, S., (IJAAEE), J. N.-I. J. A. A. E. E., & 2017, U. (2017). Approach to Quantify Groundwater Recharge Using GIS Based Water Balance Model: A Review. *International Journal of Research in Chemical, Metallurgical and Civil Engineering*, *4*(1). https://doi.org/10.15242/ijrcmce.ae0317115

45. Salati, E., Dall'Olio, A., Matsui, E., & Gat, J. R. (1979). Recycling of water in the Amazon Basin: An isotopic study. Water Resources Research, *15*(5), 1250–1258. https://doi.org/10.1029/WR015i005p01250
46. Scanlon, B. R., Healy, R. W., & Cook, P. G. (2002). Choosing appropriate techniques for quantifying groundwater recharge. Hydrogeology Journal, *10*(1), 18–39. https://doi.org/10.1007/s10040-001-0176-2
47. Terada, R., Hirata, R., Galvão, P., Saraiva, F., Tasse, N., Luiz, M., & Conicelli, B. (2022). Hydraulic relationship between aquifer and pond under potential influence of eucalyptus and sugarcane in tropical region of São Paulo, Brazil. Environmental Earth Sciences, *81*(9). https://doi.org/10.1007/s12665-022-10349-1
48. Thornthwaite, C. W., & Mather, J. R. (1955). The water balance. Laboratory of Climatology Report No. 8. *Drexel Institute of Technology*, *New Jersey, USA*.
49. Torracchi, J. (2015). *Deforestación y Pérdida de hábitat en Bosques de montaña en la Cuenca alta del Río Zamora (Loja, Ecuador)*. https://dialnet.unirioja.es/servlet/tesis?codigo=116354
50. Tropical Rainfall Measuring Mission (TRMM). (2011). *TRMM (TMPA) Rainfall Estimate L3 3 hour 0.25 degree x 0.25 degree V7*. Goddard Earth Sciences Data and Information Services Center (GES DISC). https://doi.org/10.5067/TRMM/TMPA/3H/7
51. van Teijlingen, K., & Hogenboom, B. (2016). Debating Alternative Development at the Mining Frontier: Buen Vivir and the Conflict around El Mirador Mine in Ecuador. Journal of Developing Societies, *32*(4), 382–420. https://doi.org/10.1177/0169796X16667190
52. Victoria, R. L., Martinelli, L. A., Mortatti, J., & Richey, J. (1991). Mechanisms of water recycling in the Amazon basin: isotopic insights. Ambio, *20*(8), 384–387. https://doi.org/10.2307/4313869
53. Villa-Achupallas, M., Rosado, D., Aguilar, S., & Galindo-Riaño, M. D. (2018). Water quality in the tropical Andes hotspot: The Yacuambi river (southeastern Ecuador). Science of the Total Environment, *633*, 50–58. https://doi.org/10.1016/j.scitotenv.2018.03.165
54. Wood, W. W. (1999). Use and misuse of the chloride-mass balance method in estimating ground water recharge. In *Ground Water* (Vol. 37, Issue 1, pp. 2–3). National Ground Water Association. https://doi.org/10.1111/j.1745-6584.1999.tb00949.x
55. Yeh, H. F., Lin, H. I., Lee, C. H., Hsu, K. C., & Wu, C. S. (2014). Identifying seasonal groundwater recharge using environmental stable isotopes. Water (Switzerland), *6*(10), 2849–2861. https://doi.org/10.3390/w6102849
56. Yeh, H. F., Lin, H. I., Lee, S. T., Chang, M. H., Hsu, K. C., & Lee, C. H. (2014). GIS and SBF for estimating groundwater recharge of a mountainous basin in the Wu River watershed, Taiwan. Journal of Earth System Science, *123*(3), 503–516. https://doi.org/10.1007/s12040-014-0420-5
57. Yin, L., Hou, G., Su, X. S., Wang, D., Dong, J., Hao, Y., & Wang, X. (2011). Isotopes (δD and δ18O) in precipitation, groundwater and surface water in the Ordos Plateau, China: Implications with respect to groundwater recharge and circulation. Hydrogeology Journal, *19*(2), 429–443. https://doi.org/10.1007/S10040-010-0671-4

Figures

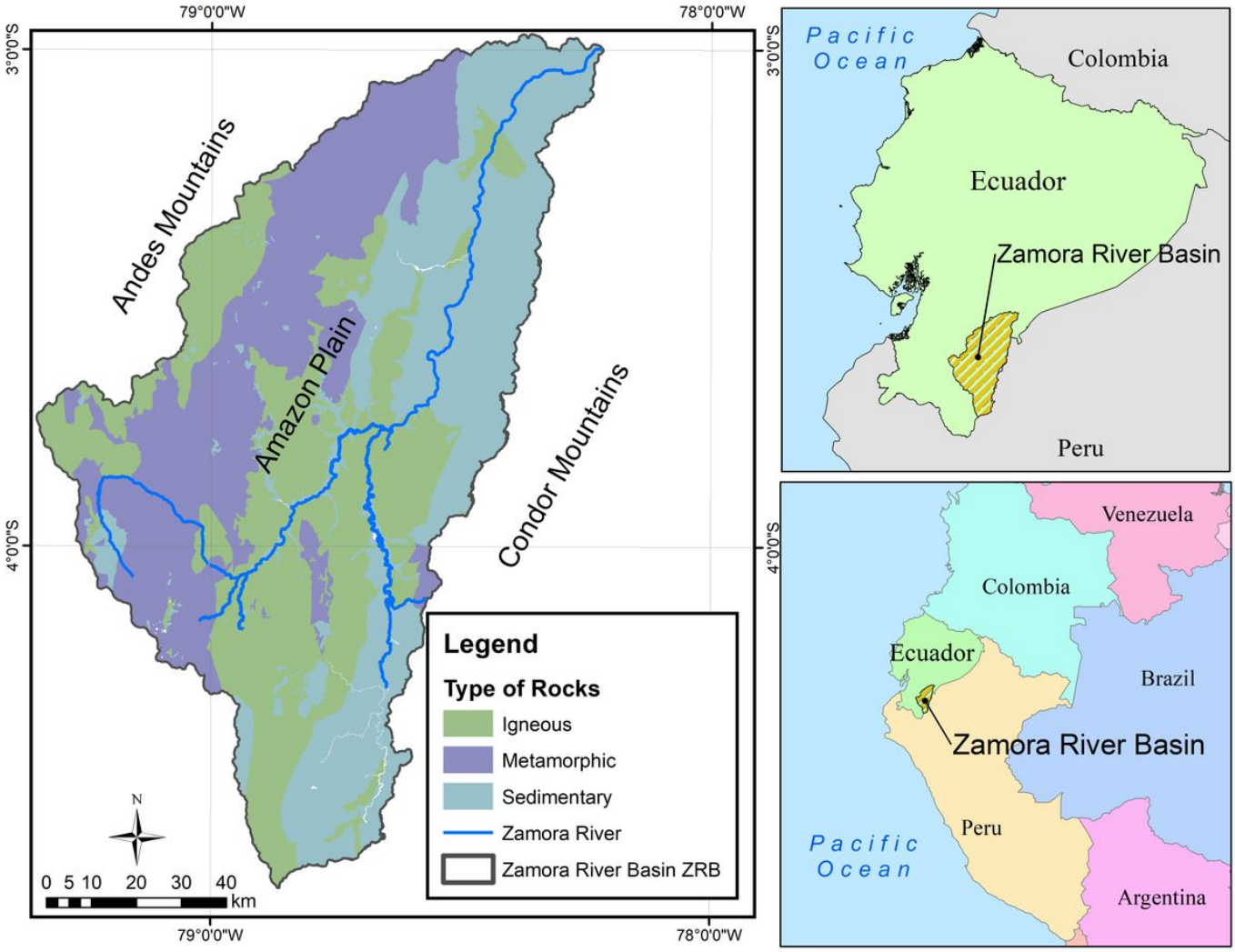

Figure 1

Location of Zamora River Basin showing the main geology units of ZRB and main sections of Zamora River.

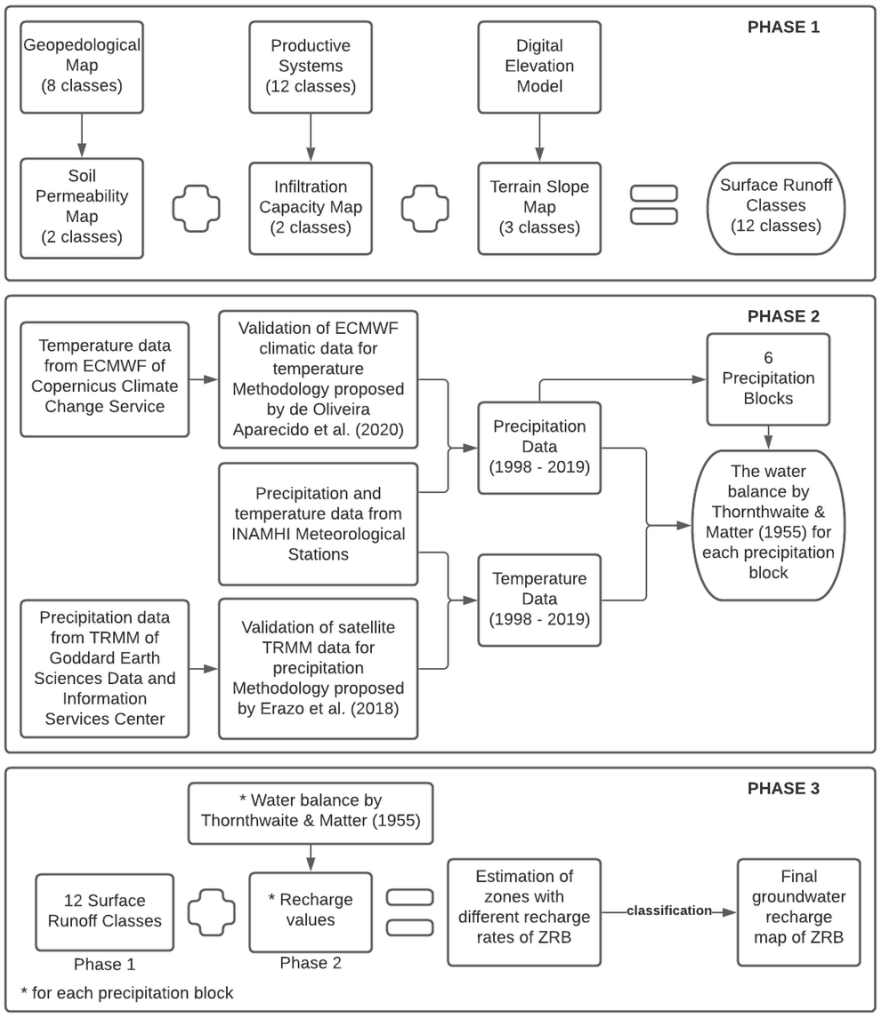

Figure 2

Methodological scheme used to estimate the groundwater recharge in ZRB with the GIS-based index model. Phase 1: Establish the surface runoff classes of the basin soil. Phase 2: Establish the precipitation blocks (basin areas with similar precipitation values), treatment and validation of meteorological and reanalysis data, and the respective Thornthwaite & Mather (1955) water balance for each precipitation block to obtain groundwater recharge values. Phase 3: spatial distribution of the groundwater recharge values from the water balance (phase 2) to the surface runoff classes (phase 1) and its classification according to ratios.

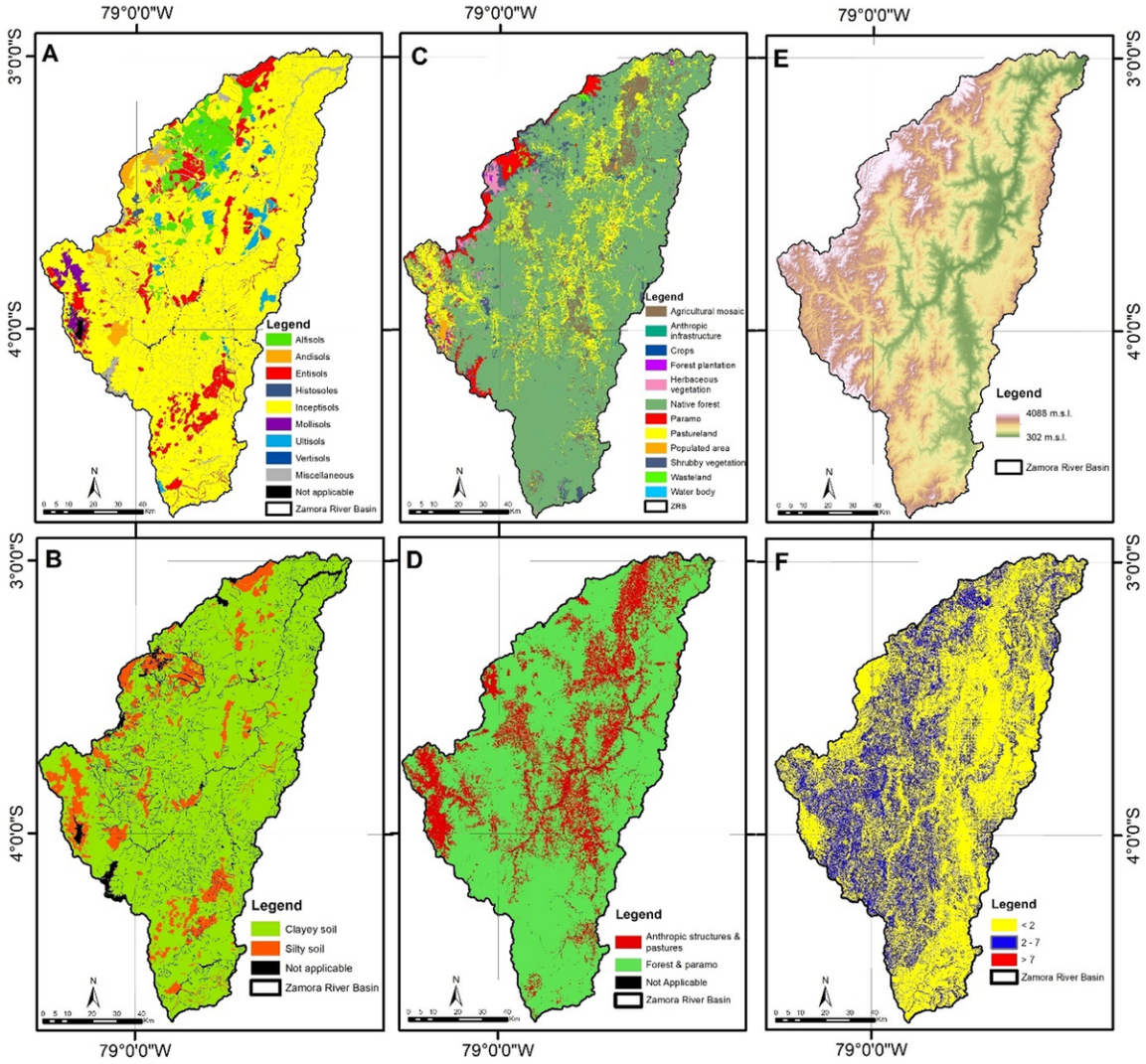

Figure 3

Soil taxonomic classification of Zamora River Basin ZRB (A) and the distribution of soil permeability classes (B). Land cover of Zamora River Basin ZRB (C) and distribution of infiltration capacity classes (D). Digital Elevation Model of Zamora River Basin ZRB (E) and the terrain slope map indicating predominance for slopes < 7 (F).

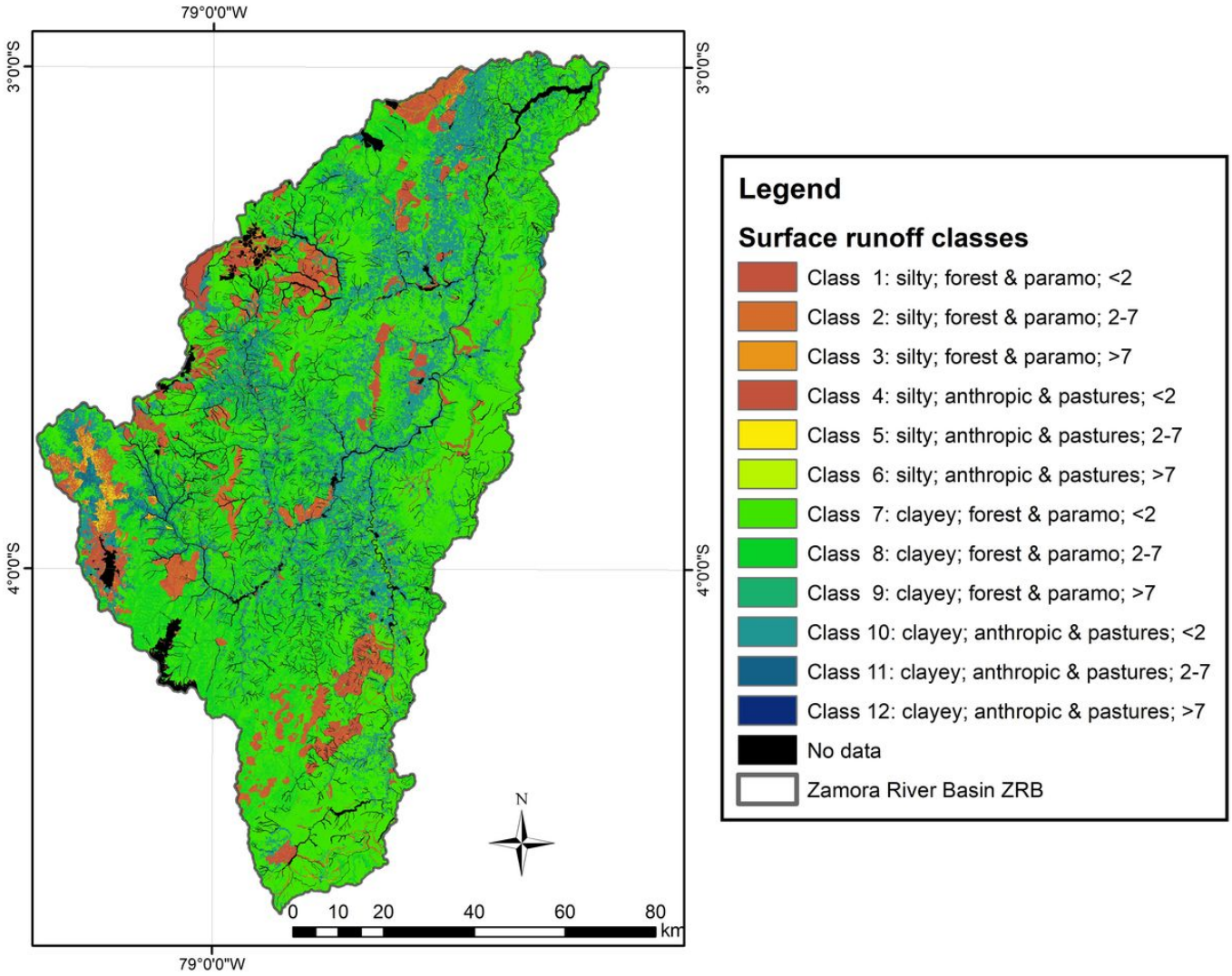

Figure 4

Final surface runoff map of the ZRB. The runoff classes result from the integration of maps of soil permeability, infiltration capacity, and terrain slope. The map shows twelve soil classes according to their capacity to generate runoff, being layer 1 the most permeable and layer 12 the least permeable.

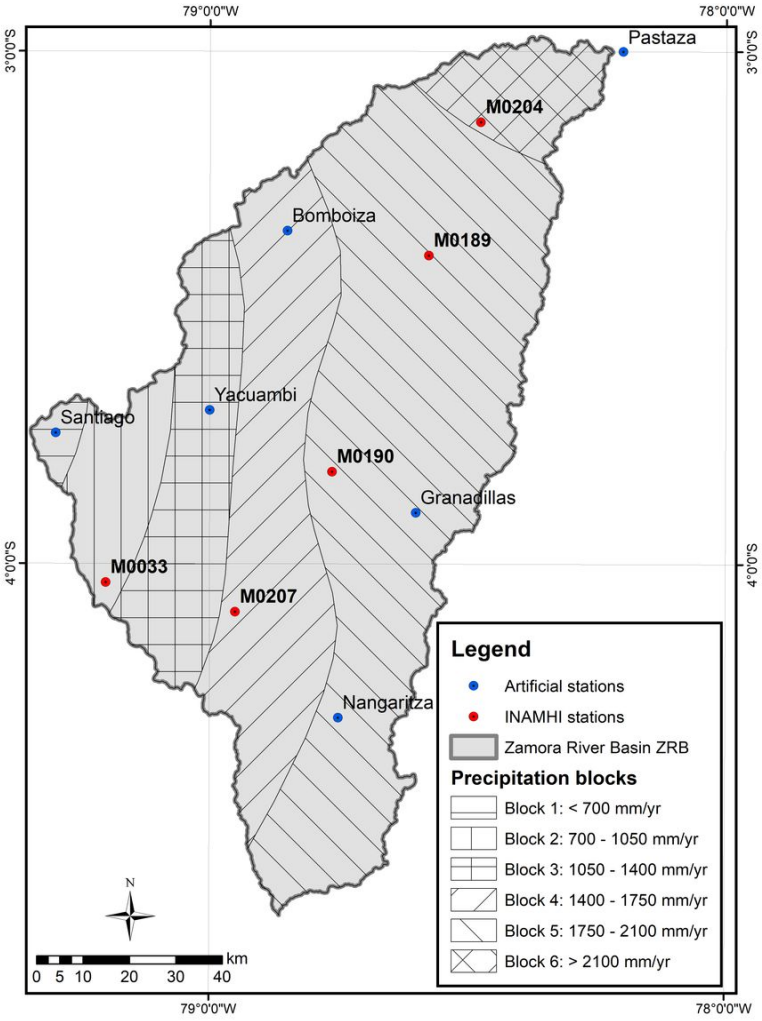

Figure 5

Precipitation blocks and location of meteorological stations for the analysis in Zamora River Basin (ZRB). Precipitation blocks represent areas where precipitation is quantitatively homogeneous throughout the year.

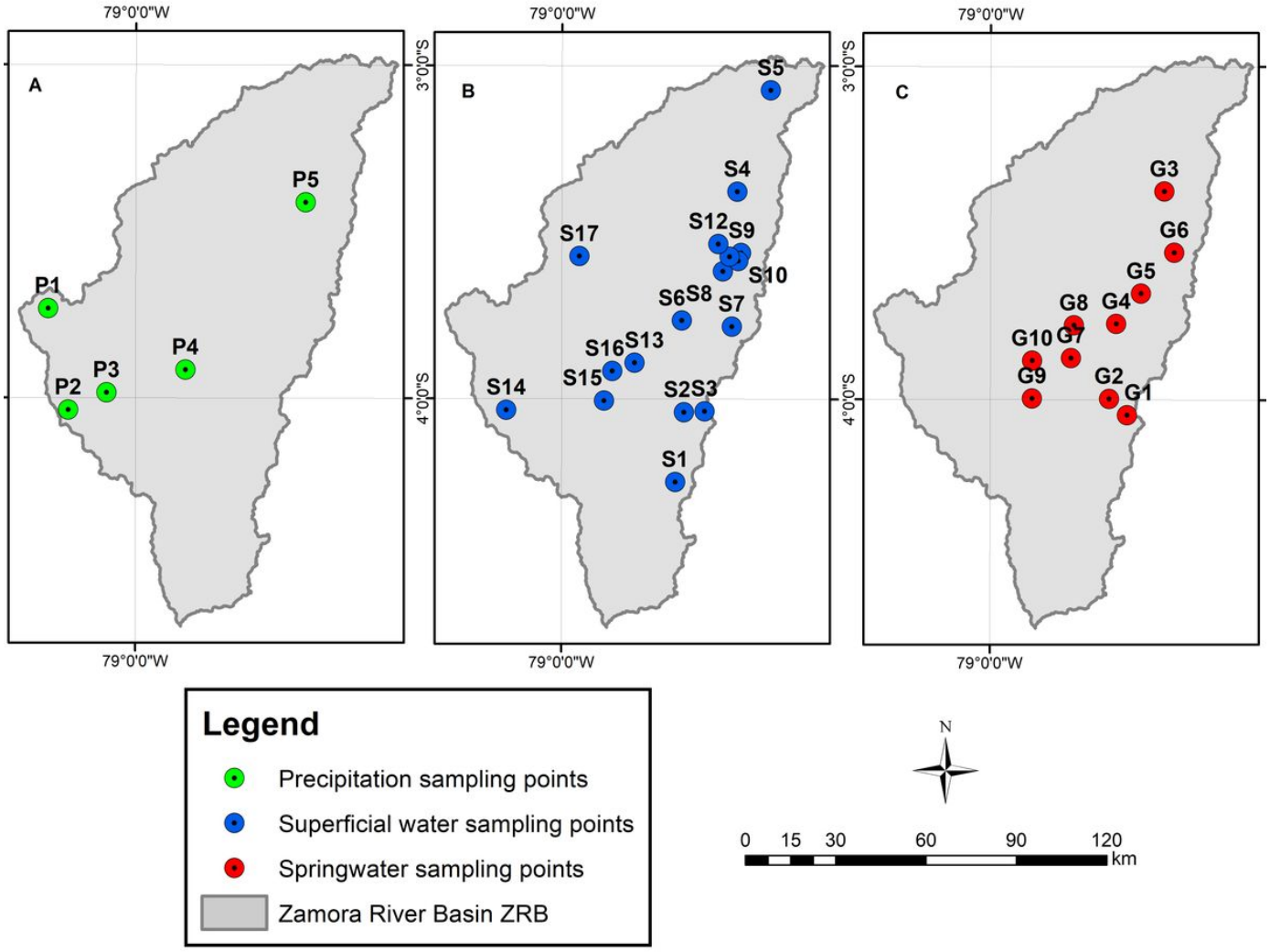

Figure 6

Sampling sites of $\delta^{18}O$ and $\delta^{2}H$ in Zamora River Basin (ZRB). Precipitation samples (A), surface water samples (B), and spring water samples (C). All sampling sites were visited in both sampling campaigns, in January for the rainy season and in September for the dry season.

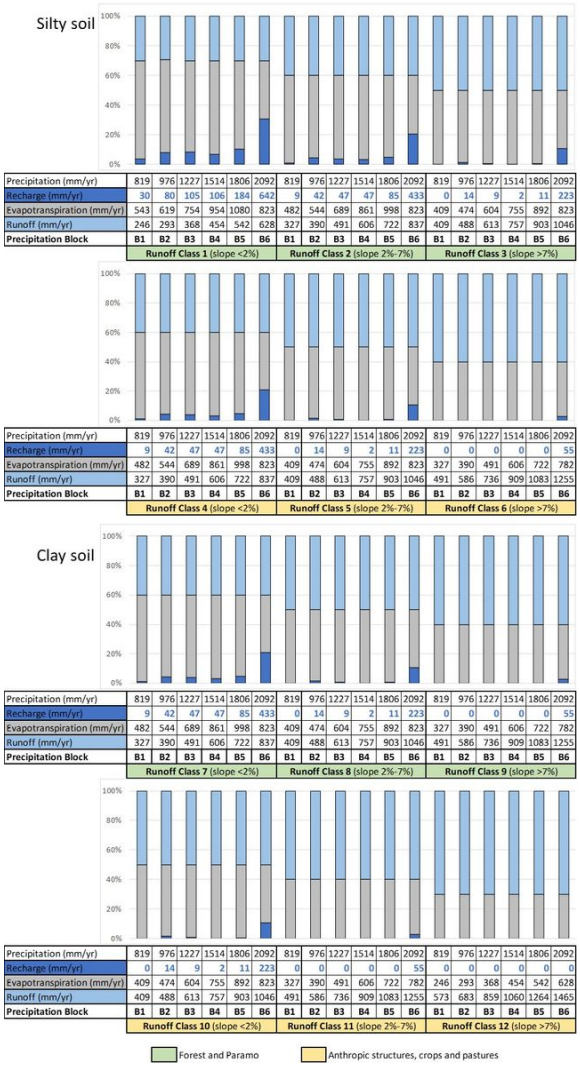

Figure 7

Results of water balances conducted for different precipitation blocks and runoff classes in the Zamora River Basin (ZRB). The precipitation blocks are labeled as B1 to B6, and the runoff classes are divided into silty and clay soils, with forest/paramo cover labeled in green and anthropic structures/crops/pastures labeled in yellow. The table highlights the groundwater recharge values for each runoff class in every precipitation block, marked in blue.

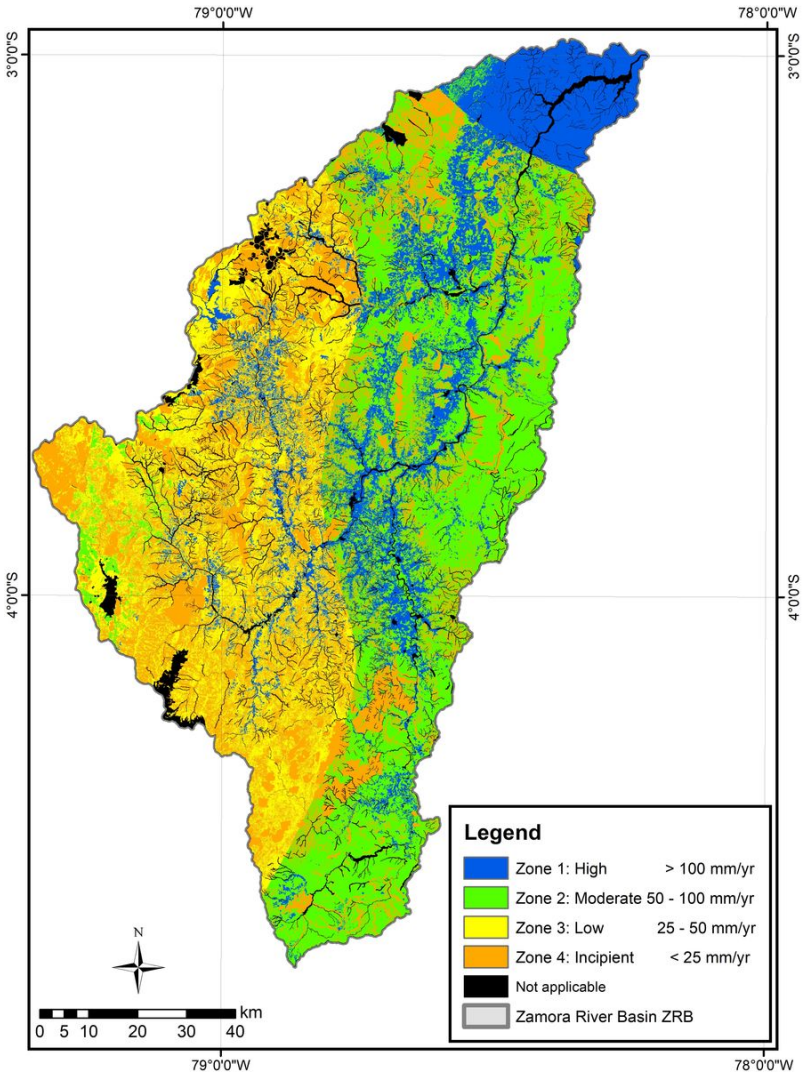

Figure 8

Final groundwater recharge map of Zamora River Basin. Zone 1 is mainly in the north of the basin, in some patches of precipitation zone 5 and in the areas close to rivers of the rest of the basin. Zone 2 extends mainly over what corresponds to precipitation zone 5, although there are also patches in precipitation block 2. Zone 3 is mainly concentrated in what corresponds to precipitation blocks 2, 3 and 4. Zone 4 covers patches of almost the entire basin, mainly in the western part of the basin.

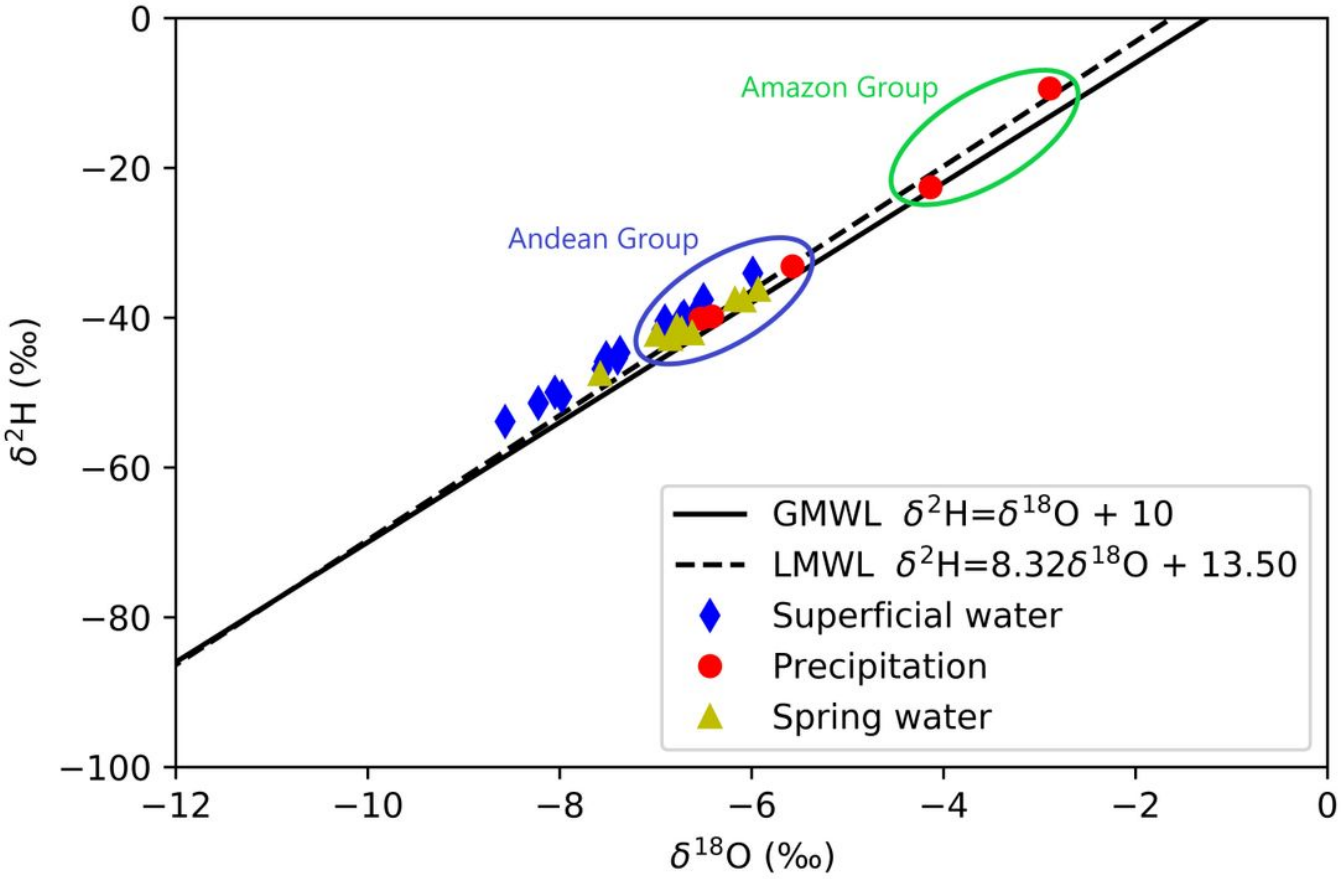

Figure 9

LMWL and the relationship between $\delta^{18}O$ and δ^2H in precipitation, superficial water, and spring water in Zamora River Basin (ZRB). The precipitation samples were classified into two groups according to isotopic characteristics, the Amazonian group characterized by isotope content that shows that they have undergone recycling processes and the Andean group that has isotopic characteristics of having influence from the Pacific coast of Ecuador.

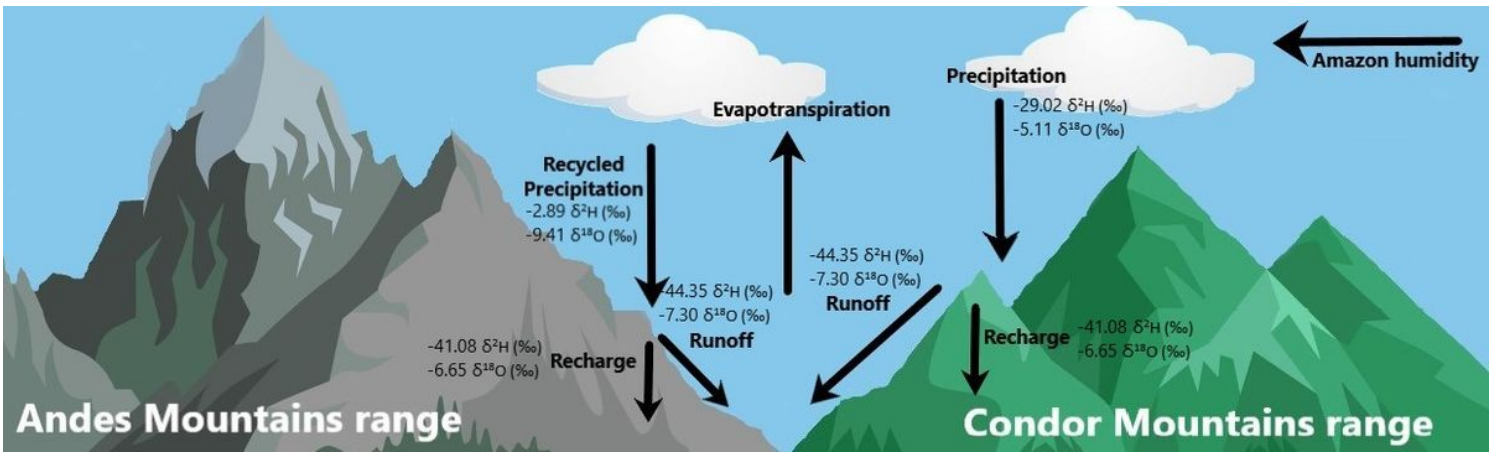

Figure 10

Scheme of the groundwater recharge in a conceptual model for ZRB and the mean isotopic composition samples of groundwater, superficial water and precipitation.